MIXED NOISE REMOVAL IN HYPERSPECTRAL IMAGES USING LOW-RANK TENSOR DECOMPOSITION WITH SPATIAL-SPECTRAL WEIGHTED SPARSITY REGULARIZATION

Hanh T. M. Tran, Tung Thanh Huynh, Thanh Van Vu, Tran Dang Khoa Phan*

The University of Danang - University of Science and Technology, Vietnam

*Corresponding author: ptdkhoa@dut.udn.vn

(Received: May 05, 2025; Revised: June 18, 2025; Accepted: June 21, 2025)

DOI: 10.31130/ud-jst.2025.23(9C).538E

Abstract - This paper addresses the problem of hyperspectral image (HSI) restoration under mixed noise, specifically Gaussian and impulse noise, by proposing a novel method based on low-rank tensor decomposition. While existing low-rank approaches often adopt fixed regularization schemes, they may fail to capture spatial-spectral correlations in HSIs. To overcome this limitation, we introduce a spatial-spectral adaptive model that integrates regularizers with pixel-wise weighting, enabling local structural preservation and improved denoising performance. An efficient optimization algorithm based on the Augmented Lagrangian Method (ALM) is developed, with closed-form solutions derived for subproblems to ensure both accuracy and convergence. Experimental results on both simulated and real HSI datasets demonstrate the superiority of the proposed method over several state-of-the-art approaches, which are based on low-rank tensor decomposition. Our method achieves higher PSNR, SSIM, and FSIM scores, and provides visually cleaner results with better preservation of image details.

Key words – Hyperspectral image restoration, low-rank tensor decomposition, group sparsity, mixed noise.

1. Introduction

A hyperspectral image (HSI) is a type of image that captures continuous spectral information across hundreds of narrow wavelength bands for each pixel, enabling detailed analysis of material composition in a scene. Its advantages include the ability to distinguish materials with similar spectral properties, with applications in precision agriculture, environmental monitoring, biomedical imaging, and military target identification. HSIs are often affected by noise due to various environmental factors during acquisition. Common types of noise include impulse noise, Gaussian noise, and dead pixels. Such noise degrades image quality and negatively impacts subsequent processing steps like classification or detection. Therefore, restoring HSIs is essential to ensure accurate analysis and interpretation.

In this paper, we investigate the problem of restoring hyperspectral images corrupted by mixed noise, which is a mixture of Gaussian and impulse noise. Several studies have focused on denoising mixed noise in HSIs to improve image quality for subsequent analysis. HSIs have strong relationships in both the spatial and spectral domains. Nearby pixels often share similar spectral features, and the spectral bands are closely related to each other. Because of that, it's important to use methods that take advantage of both spatial and spectral information. Some suitable approaches include spectral–spatial filters, low-rank models, or methods that combine both domains.

Variational methods are widely used in HSI restoration thanks to their ability to incorporate prior assumptions and regularization into an optimization framework. Total variation is commonly applied to remove noise while preserving object edges. Spatial–spectral adaptive total variation models were proposed that performs well on mixed noise [1-5]. Among various restoration techniques, non-local filtering has gained attention due to its ability to exploit the self-similarity of image patches across both spatial and spectral dimensions. Sippel et al. [6] proposed a non-local filtering method for HSI reconstruction by finding similar patches and applying collaborative Wiener filtering.

Dimensionality reduction techniques play an important role in HSI denoising by simplifying the data while preserving essential spectral information. Some studies applied Principal Component Analysis (PCA) for HSI restoration by reducing dimensionality and removing noise in the less significant components. Qian et al. [7] proposed a PCA-based method combined with spatial filtering to suppress noise and enhance image quality.

HSIs often have a low-rank structure because of the strong correlation between spectral bands. Therefore, low-rank decomposition methods can effectively separate noise from the main information, making them useful for denoising [8-12]. Wang et al. [13] introduced a HSI restoration method that combines low-rank Tucker tensor decomposition with anisotropic spatial-spectral total variation regularization to effectively separate clean image structures from mixed noise. In [14], the authors used low-rank tensor approximation guided by multigraph structures to restore HSIs. Chen et al. [15] combined low-rank tensor decomposition with weighted group sparsity. The group sparsity term guides the model to treat related pixels together, which improves noise removal without losing important details.

While traditional model-based methods have shown strong performance in HSI restoration, they often struggle with real-world complexity and variability. Recently, deep learning has offered more flexible and data-driven ways to recover clean images. Deep learning methods for HSI restoration typically learn mappings from noisy to clean images using large amounts of training samples [16-19]. They often capture complex spatial-spectral patterns better than hand-crafted models, making them well-suited for real-world noise. In [20], the authors incorporated low-rank tensor priors into deep learning frameworks for

improved HSI restoration. Deep learning methods can model complex, non-linear relationships and often achieve higher restoration quality than traditional approaches like low-rank tensor decomposition, especially on large and diverse datasets. However, they usually require substantial labeled data and training time, and may generalize poorly to unseen noise types or sensor conditions.

In this paper, we focus on low-rank tensor decomposition methods for restoring HSIs corrupted by mixed noise, specifically Gaussian and impulse noise. Most existing low-rank tensor decomposition methods rely on fixed regularization across the entire image, which may overlook local variations in spatial and spectral characteristics. This limitation highlights the need for models that can adaptively adjust to spatial-spectral structures for more accurate HSI restoration. The proposed approach incorporates group sparsity to better preserve structural consistency. To further enhance restoration quality, spatial-spectral adaptiveness is introduced through a pixel-wise weighting function embedded in the model. An optimization algorithm based on the Augmented Lagrangian Method (ALM) is developed to efficiently solve the proposed problem.

The main contributions of this study can be summarized as follows:

- We propose a novel HSI restoration model that integrates low-rank tensor decomposition with group sparsity regularization, in which the model components are adaptively weighted across spatial and spectral dimensions to better capture local variations and enhance restoration accuracy.

- An efficient optimization algorithm based on the augmented Lagrangian framework is developed to solve the resulting model, where closed-form solutions are derived for subproblems to ensure convergence and computational efficiency.

- Extensive experiments on both synthetic and real hyperspectral datasets demonstrate that the proposed method achieves superior performance compared to several state-of-the-art approaches, which employ low-rank tensor decomposition.

2. Preliminaries

2.1. Notations

A tensor is a N-way array, and N is referred to as the order of the tensor. Formally, an N-order tensor $\mathcal{X} \in \mathbb{R}^{I_1 \times I_2 \times \cdots \times I_N}$ is an array indexed by N indices, where I_n denotes the size along the n-th mode. Tensors are widely used to represent high-dimensional data, such as hyperspectral images, where the spatial and spectral dimensions are naturally modeled as a 3rd-order tensor. A fiber is a vector obtained by fixing all indices of a tensor except one. A mode-n fiber is the vector obtained by varying the n-th index while keeping the others fixed. A slice is a two-dimensional section of a tensor, obtained by fixing all indices except two. The n-mode product of a tensor $\mathcal{X} \in \mathbb{R}^{I_1 \times I_2 \times \cdots \times I_N}$ with a matrix $\mathbf{U} \in \mathbb{R}^{J \times I_n}$ is denoted by $\mathcal{X} \times_n \mathbf{U}$. For a comprehensive overview of tensor representations and operations, readers are referred to [21].

2.2. Problem statement

A degraded HSI is commonly affected by mixed noise, which typically includes Gaussian and impulse noise. Accordingly, the degradation model of HSI under mixed noise can be expressed as follows:

$$\mathcal{Y} = \mathcal{X} + \mathcal{S} + \mathcal{N}, \tag{1}$$

where, $\mathcal{Y}$ – the noisy image; $\mathcal{X}$ – the clean image; $\mathcal{S}$ – the sparse noise; and $\mathcal{N}$ – the Gaussian noise. The terms $\mathcal{Y}, \mathcal{X}, \mathcal{S}, \mathcal{N} \in \mathbb{R}^{m \times n \times b}$ are 3rd-order tensors, where $m \times n$ represents the spatial resolution of each band and b is the total number of spectral band. HSI restoration estimates the latent clean image $\mathcal{X}$ given the noisy image $\mathcal{Y}$.

2.3. Low-rank tensor decomposition

Low-rank tensor decomposition is a powerful tool for modeling the global structure of high-dimensional data by exploiting its inherent redundancy. Among various decomposition techniques, Tucker decomposition is one of the most widely used methods. It represents a tensor as the multilinear product of a smaller core tensor and a set of orthogonal factor matrices along each mode. Specifically, given a 3rd-order tensor $\mathcal{X} \in \mathbb{R}^{I_1 \times I_2 \times I_3}$, Tucker decomposition approximates it as:

$$\mathcal{X} \approx \mathcal{C} \times_1 \mathbf{U}_1 \times_2 \mathbf{U}_2 \times_3 \mathbf{U}_3, \tag{2}$$

where $\mathcal{C} \in \mathbb{R}^{r_1 \times r_2 \times r_3}$ is the core tensor capturing interactions between components, and $\mathbf{U}_n \in \mathbb{R}^{I_n \times r_n}$ are the factor matrices, which satisfy $\mathbf{U}_i^T \mathbf{U}_i = \mathbf{I}$. The low-rank property is imposed by choosing $r_n \ll I_n$, allowing Tucker decomposition to effectively reduce noise and preserve the essential structure of hyperspectral data. The Tucker decomposition of a 3rd-order tensor is illustrated in Figure 1.

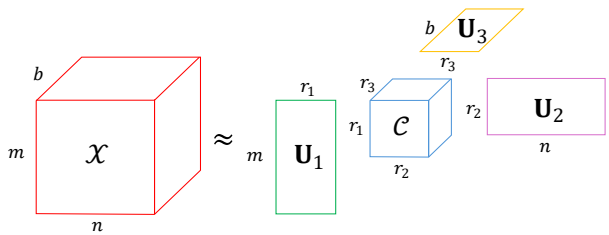

Figure 1. *Tucker decomposition of a 3rd-order tensor*

2.4. Group sparsity

In [15], Chen et al. introduced a hyperspectral image restoration model that integrates low-rank tensor decomposition with a weighted group sparsity regularization. In this framework, the group sparsity prior is applied to the sparse noise component, which is assumed to exhibit structural correlations across spectral bands. The group sparsity is defined by:

$$\begin{aligned} \|\mathbf{W} \odot D\mathcal{X}\|_{2,1} = &\sum_{i=1}^{m}\sum_{j=1}^{n} \mathbf{W}_x(i,j) \|D_x \mathcal{X}(i,j,:)\|_2 \\ &+ \sum_{i=1}^{m}\sum_{j=1}^{n} \mathbf{W}_y(i,j) \|D_y \mathcal{X}(i,j,:)\|_2, \end{aligned} \tag{3}$$

where $\mathbf{W}$ is the weight matrix; $\odot$ denotes the Hadamard product; D is the gradient operator with the two spatial

components D_x and D_y; and $\mathcal{X}(i,j,:)$ is the spectral vector at spatial location (i,j).

By grouping pixels along the spectral dimension, the method enforces sparsity at the group level rather than on individual elements, thus better capturing the continuity and joint occurrence of noise across bands.

3. Proposed model

To address the challenges of mixed noise removal in HSIs, we formulate a restoration model that leverages both the low-rank property of hyperspectral data and the structural sparsity of noise components. Specifically, the clean HSI is modeled via a low-rank Tucker decomposition to capture its global spatial-spectral correlations. In addition, group sparsity is imposed on the low-rank component to promote structured regularity, especially in local neighborhoods. To better adapt to the spatial and spectral variability across pixels, we introduce spatial-spectral weighting schemes into the regularization terms. These weights are designed to emphasize the preservation of fine structures and local textures while suppressing noise adaptively. Based on these considerations, the proposed optimization problem is formulated as follows:

$$\begin{aligned}\min_{\mathcal{X},\mathcal{S},\mathcal{C},\mathbf{U}_i,\mathcal{T},\mathcal{Z}} \lambda_1\|\mathbf{W}\odot\mathcal{T}\|_{2,1}+\lambda_2\|\mathcal{W}\odot\mathcal{S}\|_1\\ s.t.\,\mathcal{X}\approx\mathcal{C}\times_1\mathbf{U}_1\times_2\mathbf{U}_2\times_3\mathbf{U}_3,\\ \|\mathcal{Y}-\mathcal{X}-\mathcal{S}\|_F^2\le\varepsilon,\mathcal{X}=\mathcal{Z},\mathcal{T}=D\mathcal{Z},\end{aligned} \tag{4}$$

where $\mathcal{S}$ models the sparse noise; the terms $\|\mathbf{W}\odot\mathcal{T}\|_{2,1}$ and $\|\mathcal{W}\odot\mathcal{S}\|_1$ encode the adaptive group sparsity and spatial-spectral sparsity, respectively; λ_1 and λ_2 denote regularization parameters; ε is the variance of the Gaussian noise.

Following the framework of the Augmented Lagrangian Method (ALM) [22], we reformulate the constrained optimization problem as the minimization of the corresponding augmented Lagrangian function:

$$\begin{aligned}L_\beta(\mathcal{X},\mathcal{S},\mathcal{C},\mathbf{U}_i,\mathcal{T},\mathcal{Z},\mathcal{M}_i)=\lambda_1\|\mathbf{W}\odot\mathcal{T}\|_{2,1}+\\ +\lambda_2\|\mathcal{W}\odot\mathcal{S}\|_1+\langle\mathcal{M}_1,\mathcal{Y}-\mathcal{X}-\mathcal{S}\rangle\\ +\frac{\beta}{2}\|\mathcal{Y}-\mathcal{X}-\mathcal{S}\|_F^2+\langle\mathcal{M}_2,\mathcal{X}-\mathcal{Z}\rangle\\ +\frac{\beta}{2}\|\mathcal{X}-\mathcal{Z}\|_F^2+\langle\mathcal{M}_3,D\mathcal{Z}-\mathcal{T}\rangle+\frac{\beta}{2}\|\mathcal{X}-\mathcal{Z}\|_F^2\end{aligned} \tag{5}$$

under the constraint of low-rank Tucker decomposition $\mathcal{X}\approx\mathcal{C}\times_1\mathbf{U}_1\times_2\mathbf{U}_2\times_3\mathbf{U}_3$, where $\langle\cdot,\cdot\rangle$ denotes the inner product; $\mathcal{M}_i$ $(i=1,2,3)$ are the Lagrange multipliers; β denotes a penalty parameter.

To efficiently solve the unconstrained optimization problem derived from the augmented Lagrangian formulation, we adopt an alternating minimization strategy. Specifically, each variable is updated by minimizing the augmented Lagrangian function L_β with respect to one variable while keeping the others fixed. This decomposition yields a series of subproblems that are simpler and can be solved either in closed form or using efficient numerical schemes. In the following, we present the subproblems and their solutions.

- The $\mathcal{X},\mathcal{C},\mathbf{U}_i$ problem:

$$\begin{aligned}\min_{\mathcal{X}}\langle\mathcal{M}_1,\mathcal{Y}-\mathcal{X}-\mathcal{S}\rangle+\frac{\beta}{2}\|\mathcal{Y}-\mathcal{X}-\mathcal{S}\|_F^2\\ +\langle\mathcal{M}_2,\mathcal{X}-\mathcal{Z}\rangle+\frac{\beta}{2}\|\mathcal{X}-\mathcal{Z}\|_F^2,\end{aligned} \tag{6}$$

which is equivalent to:

$$\min_{\mathcal{X}}\beta\left\|\mathcal{X}-\frac{1}{2}\left(\mathcal{Y}-\mathcal{S}+\mathcal{Z}+\frac{\mathcal{M}_1-\mathcal{M}_2}{\beta}\right)\right\|_F^2, \tag{7}$$

under the constraint of $\mathcal{X}\approx\mathcal{C}\times_1\mathbf{U}_1\times_2\mathbf{U}_2\times_3\mathbf{U}_3$ with $\mathbf{U}_i^T\mathbf{U}_i=\mathbf{I}$. The higher-order orthogonal iteration (HOOI) [21] is used to compute the core tensor $\mathcal{C}$ and the factor matrices $\mathbf{U}_i$ in the Tucker decomposition. Then, the latent tensor $\mathcal{X}$ is updated.

- The $\mathcal{Z}$ problem:

$$\begin{aligned}\min_{\mathcal{Z}}\langle\mathcal{M}_2,\mathcal{X}-\mathcal{Z}\rangle+\frac{\beta}{2}\|\mathcal{X}-\mathcal{Z}\|_F^2\\ +\langle\mathcal{M}_3,D\mathcal{Z}-\mathcal{T}\rangle+\frac{\beta}{2}\|D\mathcal{Z}-\mathcal{T}\|_F^2,\end{aligned} \tag{8}$$

which leads to the following system of linear equations:

$$(\mathcal{I}+D^TD)\mathcal{Z}=\left(\mathcal{X}+\frac{\mathcal{M}_2}{\beta}\right)+D^T\left(\mathcal{T}-\frac{\mathcal{M}_3}{\beta}\right), \tag{9}$$

where $\mathcal{I}$ is the identity tensor. The above equation can be solved efficiently using fast Fourier transform (FFT) as:

$$\mathcal{Z}=\boldsymbol{\mathcal{F}}^{-1}\left\{\frac{\boldsymbol{\mathcal{F}}\left[\left(\mathcal{X}+\frac{\mathcal{M}_2}{\beta}\right)+D^T\left(\mathcal{T}-\frac{\mathcal{M}_3}{\beta}\right)\right]}{\mathbf{I}+\boldsymbol{\mathcal{F}}(D^TD)}\right\}, \tag{10}$$

where $\boldsymbol{\mathcal{F}}$ and $\boldsymbol{\mathcal{F}}^{-1}$ are FFT and inverse FFT; the division is performed element-wise.

- The $\mathcal{T}$ problem:

$$\begin{aligned}\min_{\mathcal{T}}\lambda_1\|\mathbf{W}\odot\mathcal{T}\|_{2,1}+\langle\mathcal{M}_3,D\mathcal{Z}-\mathcal{T}\rangle\\ +\frac{\beta}{2}\|D\mathcal{Z}-\mathcal{T}\|_F^2,\end{aligned} \tag{11}$$

which is equivalent to:

$$\min_{\mathcal{T}}\lambda_1\|\mathbf{W}\odot\mathcal{T}\|_{2,1}+\frac{\beta}{2}\left\|D\mathcal{Z}-\mathcal{T}+\frac{\mathcal{M}_3}{\beta}\right\|_F^2. \tag{12}$$

The closed-form solution for the tube fibers $\mathcal{T}(i,j,:)$ of $\mathcal{T}$ can be efficiently computed using the soft-threshold shrinkage operator:

$$\mathcal{T}(i,j,:)=\mathbf{Shrinkage}\left\{\mathcal{V}(i,j,:),\frac{\mathbf{W}(i,j)\lambda_1}{\beta}\right\}, \tag{13}$$

where $\mathbf{Shrinkage}(a,b)=sign(a)\,max(|a|-b,0)$; $\mathcal{V}=D\mathcal{Z}+\frac{\mathcal{W}_3}{\beta}$.

- The $\mathcal{S}$ problem:

$$\begin{aligned}\min_{\mathcal{S}}\lambda_2\|\mathcal{W}\odot\mathcal{S}\|_1+\langle\mathcal{M}_1,\mathcal{Y}-\mathcal{X}-\mathcal{S}\rangle\\ +\frac{\beta}{2}\|\mathcal{Y}-\mathcal{X}-\mathcal{S}\|_F^2,\end{aligned} \tag{14}$$

which leads to a closed-form solution using element-wise soft-thresholding as:

$$\mathcal{S}=\mathbf{Shrinkage}\left(\mathcal{Y}-\mathcal{X}+\frac{\mathcal{M}_1}{\beta},\frac{\mathcal{W}\lambda_2}{\beta}\right). \tag{15}$$

- Multiplier update:

The Lagrange multipliers are updated as follows:

$$\begin{aligned}\mathcal{M}_1 &= \mathcal{M}_1 + \beta(\mathcal{Y} - \mathcal{X} - \mathcal{S}),\\ \mathcal{M}_2 &= \mathcal{M}_2 + \beta(\mathcal{X} - \mathcal{Z}),\\ \mathcal{M}_3 &= \mathcal{M}_3 + \beta(D\mathcal{Z} - \mathcal{T}).\end{aligned} \tag{16}$$

- The weight matrix $\mathbf{W}$ and the weight tensor $\mathcal{W}$:

$$\mathbf{W} = \frac{1}{\left\|\left(D\mathcal{Z} + \frac{\mathcal{M}_3}{\beta}\right)(i,j,:)\right\|_F^2 + \text{eps}}, \tag{17}$$

$$\mathcal{W} = \alpha_0 + \alpha_1\left[1 - \exp\left(-\frac{1}{\left\|\mathcal{Y} - \mathcal{X} + \frac{\mathcal{M}_1}{\beta}\right\|_F + \text{eps}}\right)\right], \tag{18}$$

where α_0 and α_1 are positive parameters; eps is a small positive constant used for numerical stability.

The weight matrix $\mathbf{W}$ allows the model to adaptively preserve important image structures, such as edges, textures, or regions with rich spectral information, by assigning them smaller weights, while reducing the noise by assigning larger weights. The tensor $\mathcal{W}$ is designed to adaptively control the sparsity regularization strength applied to the sparse noise component. It assigns weights based on the discrepancy between the observed data $\mathcal{Y}$ and the current estimate of the clean image $\mathcal{X}$, adjusted by the Lagrange multiplier $\mathcal{M}_1$. When the residual is large, it indicates a significant difference between the observation and reconstruction, possibly due to strong noise like impulse noise. In this case, $\mathcal{W} \approx \alpha_0$, leading to a small weight. This allows noise to be absorbed into the sparse noise $\mathcal{S}$. When the residual is small, it indicates the presence of weak noise. In this case, $\mathcal{W}$ approaches $\alpha_0 + \alpha_1$, resulting in stronger sparsity enforcement for the sparse noise component. α_0 ensures a minimum regularization effect, while α_1 controls how much stronger the penalty becomes for weak noise. The optimal values allow the model to effectively suppress noise without over-penalizing valid signal components.

The overall algorithm is summarized in Algorithm 1 as follows.

Algorithm 1. The ALM algorithm for solving the proposed model (4)

Input: $\mathcal{Y}, \lambda_1, \lambda_2, \beta, \alpha_0, \alpha_1$, and rank of the core tensor

Initialization: $\mathcal{X} = \mathcal{Y}, \mathbf{W} = \mathbf{0}$,

$$\mathcal{Z} = \mathcal{W} = \mathcal{M}_1 = \mathcal{M}_2 = \mathcal{M}_3 = 0.$$

While *the stopping criterion* is not satisfied **do**

1: Solve the $\mathcal{X}, \mathcal{C}, \mathbf{U}_i$ problem via (7).

2: Solve the $\mathcal{Z}$ problem via (10).

3: Solve the $\mathcal{T}$ problem via (13) and (17).

4: Solve the $\mathcal{S}$ problem via (15) and (18).

5: Update the multipliers $\mathcal{M}_1, \mathcal{M}_2, \mathcal{M}_3$ via (16).

6: Check the stopping criterion:

$$(\|\mathcal{X}^{k+1} - \mathcal{X}^k\|_F / \|\mathcal{X}^k\|_F) \le \tau.$$

end

4. Experimental results

4.1. Numerical experiments

To evaluate the effectiveness of the proposed method, we compare it with two representative low-rank tensor decomposition-based approaches: LRTDTV [13], which incorporates spatial-spectral total variation regularization, and LRTDGS [15], which integrates group sparsity into the decomposition model. The parameters of all the methods were tuned to achieve the best average PSNR performance. For the proposed method, several parameters were empirically fixed, including $\beta = 0.01, \alpha_0 = 0.5, \alpha_1 = 2$.

In the numerical experiments, two datasets, Washington DC Mall [23] and simulated Indian Pines [13], are used. The simulated Indian Pines dataset has a size of $145 \times 145 \times 224$, while the Washington DC Mall dataset has a size of 256×256×191. Mixed noise, including Gaussian noise and impulse noise, is added to each spectral band. For each band, the variance of the Gaussian noise is randomly selected within the range $[0, 0.2]$, and the impulse noise is introduced with a randomly chosen ratio within the range $[0, 0.2]$.

Table 1. *PSNR, SSIM and FSIM results of different methods for the simulated Indian Pines and Washington DC Mall datasets*

		LRTDTV	LRTDGS	Ours
Simulated Indian Pines	PSNR	41.25	42.92	**43.54**
	SSIM	0.9936	0.9965	**0.9974**
	FSIM	0.993	0.9969	**0.998**
Washington DC Mall	PSNR	45.5	46.8	**47.46**
	SSIM	0.9646	0.9629	**0.9781**
	FSIM	0.9398	0.9315	**0.9561**

Quantitative results in terms of PSNR, SSIM [24], and FSIM [25] on two benchmark hyperspectral datasets, Simulated Indian Pines and Washington DC Mall, are presented in Table 1. For the Simulated Indian Pines dataset, our method achieves the highest PSNR value of 43.54, outperforming LRTDGS (42.92) and LRTDTV (41.25) by noticeable margins. Similarly, in terms of structural similarity, our method achieves an SSIM of 0.9974, exceeding both LRTDGS (0.9965) and LRTDTV (0.9936). The FSIM score, which reflects perceptual image quality, is also the highest for our method (0.998), indicating superior preservation of spatial and spectral structures. In the case of the Washington DC Mall dataset, a similar trend is observed.

The PSNR, SSIM and FSIM indices are shown for all bands in Figure 2. It can be seen that the proposed method consistently achieves higher evaluation values across the majority of spectral bands compared to both LRTDTV and LRTDGS. While all three methods exhibit certain fluctuations due to varying levels of noise and structural complexity across bands, our method demonstrates superior robustness. The trends observed across PSNR, SSIM, and FSIM show a strong correlation, indicating that improvements in signal fidelity are consistently accompanied by gains in both structural and perceptual similarity. Moreover, although LRTDGS generally performs better than LRTDTV in all three metrics, its

relative performance varies more across bands. This suggests that while group sparsity improves signal recovery globally, it may not fully preserve local perceptual details without further adaptation, which emphasizes the added value of the proposed adaptive strategy.

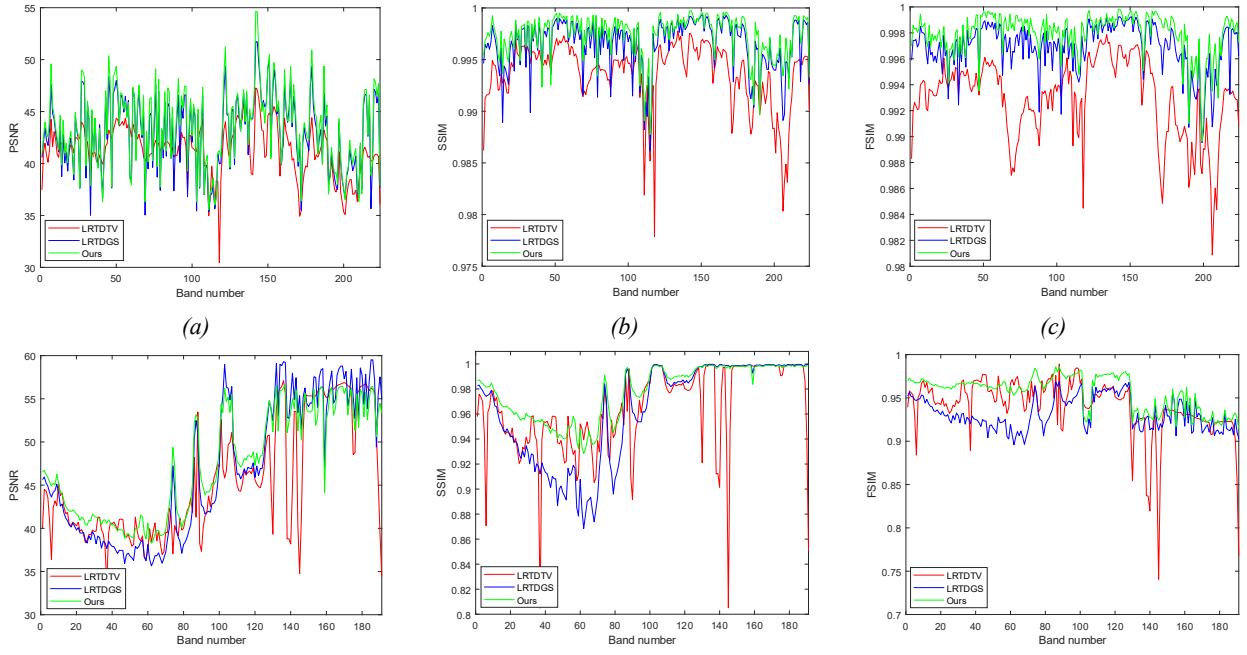

Figure 2. *PSNR, SSIM and FSIM results of all bands for different methods: (a)-(c) the simulated Indian Pines; (d)-(f) - the Washington DC Mall*

To further validate the effectiveness of the proposed method, we present a visual comparison of the denoising results on a representative band of the simulated Indian Pines and Washington DC Mall datasets, as shown in Figures 3 and 4. For better visualization, zoom-in regions are highlighted with green boxes. LRTDTV, which exploits total variation regularization, is able to reduce a portion of the noise while preserving edges to some extent. However, it tends to over-smooth homogeneous regions and introduces blocky artifacts. LRTDGS, which incorporates group sparsity constraints, performs better in preserving local structures compared to LRTDTV. Yet, some residual noise and detail blurring remain noticeable, especially along edges and in textured regions. In contrast, our proposed method achieves the most visually pleasing result. It not only suppresses noise more effectively but also maintains fine structural details and edge continuity. This improvement can be attributed to the pixel-wise adaptive weighting mechanism embedded in the model, which allows the model to dynamically adjust its regularization strength according to local spatial-spectral content.

Figure 3. *Denoising results of different methods for the band 118 of the simulated Indian Pines dataset: (a) Original; (b) Noisy; (c) LRTDTV; (d) LRTDGS; (e) Ours*

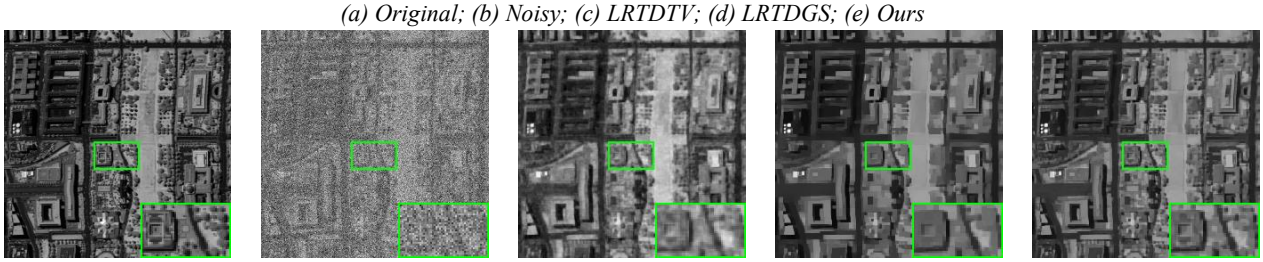

Figure 4. *Denoising results of different methods for band 95 of the Washington DC Mall dataset: (a) Original; (b) Noisy; (c) LRTDTV; (d) LRTDGS; (e) Ours*

4.2. Real experiments

To further validate the practical applicability of the proposed method, we conducted experiments on a real HSIs from the real Indian Pines dataset. The denoising results of different methods on the band 150 are shown in Figure 5. As shown in Figure 5(a), the original band 150 suffers from heavy noise corruption, with most structural and textural content overwhelmed. Since a clean reference for this band is not available, we provide band 140 as a visual reference for qualitative assessment due to its similar spatial structure. The denoising results obtained by different methods are presented in Figure 5(c)-(e).

The LRTDTV method suppresses part of the noise but exhibits noticeble over-smoothing and blurred textures, particularly in homogeneous areas. LRTDGS achives improved preservation of edge information and textures by leveraging group sparsity, yet some residual noise and visual artifacts are still evident. Our proposed method produces the cleanest visual outcome, closely resembling the structural patterns seen in the reference band. It effectively removes noise while retaining fine spatial details and contrast.

(a) *(b)* *(c)* *(d)* *(e)*

Figure 5. *Denoising results of different methods for the band 150 of real Indian Pines dataset: (a) Original; (b) Band 140 for reference; (c) LRTDTV; (d) LRTDGS; (e) Ours*

5. Conclusion

In this paper, we presented a novel low-rank tensor decomposition framework for HSI restoration under mixed noise conditions, including Gaussian and impulse noise. Unlike existing methods with fixed regularization, our model introduces spatial-spectral adaptiveness via a pixel-wise weighting strategy, enabling better modeling of local variations. To enhance structural preservation, group sparsity regularization is incorporated into the model. An efficient optimization algorithm based on the Augmented Lagrangian Method was developed, with closed-form solutions to subproblems ensuring computational feasibility. Experimental results on both simulated and real datasets demonstrate that the proposed method consistently outperforms state-of-the-art approaches such as LRTDTV and LRTDGS in terms of PSNR, SSIM, and FSIM. Visual comparisons further confirm the method's effectiveness in detail preservation and noise suppression. These results validate the benefit of adaptive regularization in HSI restoration and highlight the importance of integrating local spatial-spectral priors into low-rank models.

Acknowledgments: This work was supported by The Murata Science Foundation and The University of Danang - University of Science and Technology, code number of Project: T2024-02-03MSF.

REFERENCES

[1] Q. Yuan, L. Zhang and H. Shen, "Hyperspectral Image Denoising Employing a Spectral–Spatial Adaptive Total Variation Model", *IEEE Transactions on Geoscience and Remote Sensing*, vol. 50, no. 10, 2012, pp. 3660–3677.

[2] S. Takeyama, S. Ono and I. Kumazawa, "Hyperspectral image restoration by hybrid spatio-spectral total variation", in *Proceedings of IEEE International Conference on Acoustics, Speech and Signal Processing (ICASSP),* New Orleans, LA, USA, 2017, pp. 4586-4590.

[3] P. T. D. Khoa and T. T. H. Yen, "Edge coherence-weighted second-order variational model for image denoising", *Signal, Image and Video Processing,* vol. 16, no. 8, pp. 2313-2320, 2022.

[4] M. Wang, Q. Wang, J. Chanussot and D. Hong, "$\ell_0 - \ell_1$ hybrid total variation regularization and its applications on hyperspectral image mixed noise removal and compressed sensing", *IEEE Transactions on Geoscience and Remote Sensing*, vol. 59, no. 9, pp. 7695-7710, 2021.

[5] P. T. D. Khoa and T. T. H. Yen, "A space-variant nonlinear algorithm for denoising omnidirectional images corrupted by poisson noise", *IEEE Signal Processing Letters*, vol. 27, pp. 535-539, 2020.

[6] F. Sippel, J. Seiler and A. Kaup, "Hyperspectral Image Reconstruction from Multispectral Images Using Non-Local Filtering", in Proceedings of *IEEE 23rd International Workshop on Multimedia Signal Processing (MMSP)*, Tampere, Finland, 2021, pp. 1-6.

[7] G. Chen and S. -E. Qian, "Hyperspectral Image Denoising Using Principal Component Analysis and Wavelet Shrinkage", *IEEE Transactions on Geoscience and Remote Sensing*, vol. 50, no. 10, pp. 3717–3726, 2013.

[8] Y. Yang, Y. Feng, J. Zhang and S. Chen, "Hyperspectral image restoration via subspace-based nonlocal low-rank tensor approximation", *IEEE Geoscience and Remote Sensing Letters*, vol. 19, pp. 1-5, 2022.

[9] P. Liu, L. Liu and L. Xiao, "A novel tensor-based hyperspectral image restoration method with low-rank modeling in gradient domains", *IEEE Journal of Selected Topics in Applied Earth Observations and Remote Sensing*, vol. 16, pp. 581-597, 2022.

[10] D. Li, D. Chu, X. Guan, W. He and H. She, "Adaptive regularized low-rank tensor decomposition for hyperspectral image denoising and destriping", *IEEE Transactions on Geoscience and Remote Sensing*, vol. 62, pp. 1-17, 2024.

[11] N. Liu, L. Li, W. Li, R. Tao, J. E. Fowler and J. Chanussot, "Hyperspectral restoration and fusion with multispectral imagery via low-rank tensor-approximation", *IEEE Transactions on Geoscience and Remote Sensing,* vol. 59, no. 9, pp. 7817-7830, 2021.

[12] Y. -Y. Liu, X. -L. Zhao, Y. -B. Zheng, T. -H. Ma and H. Zhang, "Hyperspectral image restoration by tensor fibered rank constrained optimization and plug-and-play regularization", *IEEE Transactions on Geoscience and Remote Sensing*, vol. 60, pp. 1-17, 2021.

[13] Y. Wang, J. Peng, Q. Zhao, Y. Leung, X. -L. Zhao and D. Meng, "Hyperspectral image restoration via total variation regularized low-rank tensor decomposition", *IEEE Journal of Selected Topics in Applied Earth Observations and Remote Sensing*, vol. 11, no.4, pp. 1227-1243, 2017.

[14] N. Liu, W. Li, R. Tao, Q. Du and J. Chanussot, "Multigraph-based low-rank tensor approximation for hyperspectral image restoration", *IEEE Transactions on Geoscience and Remote Sensing*, vol. 60, pp. 1-14, 2022.

[15] Y. Chen, W. He, N. Yokoya and T. -Z. Huang, "Hyperspectral image restoration using weighted group sparsity-regularized low-rank tensor decomposition", *IEEE Transactions on Cybernetics*, vol. 50, no. 8, pp. 3556-3570, 2019.

[16] M. Li, Y. Fu, T. Zhang and G. Wen, "Supervise-assisted self-supervised deep-learning method for hyperspectral image restoration", *IEEE Transactions on Neural Networks and Learning Systems*, vol. 36, no. 4, pp. 7331-7344, 2025.

[17] Y. Qian, H. Zhu, L. Chen and J. Zhou, "Hyperspectral image restoration with self-supervised learning: A two-stage training approach", *IEEE Transactions on Geoscience and Remote Sensing*, vol. 60, pp. 1-17, 2021.

[18] Z. Lai, K. Wei, Y. Fu, "Deep plug-and-play prior for hyperspectral image restoration", *Neurocomputing*, vol. 481, pp. 281-293, 2022.

[19] M. Li, Y. Fu, J. Liu and Y. Zhang, "Pixel adaptive deep unfolding transformer for hyperspectral image reconstruction", in *Proceedings of the IEEE/CVF International Conference on Computer Vision,* Paris, France, 2023, pp. 12913-12922.

[20] S. Zhang, L. Wang, L. Zhang and H. Huang, "Learning tensor low-rank prior for hyperspectral image reconstruction", in *Proceedings of the IEEE/CVF Conference on Computer Vision and Pattern Recognition,* Nashville, TN, USA, 2021, pp. 12001-12010.

[21] T. G. Kolda and W. B. Brett, "Tensor decompositions and applications", *SIAM review*, vol. 51, no. 3, pp. 455-500, 2009.

[22] Z. Lin, C. Minming and M. Yi, "The augmented lagrange multiplier method for exact recovery of corrupted low-rank matrices", *Journal of Structural Biology*, vol. 181, no. 2, pp. 116-127, 2010.

[23] H. Zhang, W. He, L. Zhang, H. Shen and Q. Yuan, "Hyperspectral image restoration using low-rank matrix recovery", *IEEE Transactions on Geoscience and Remote Sensing*, vol. 52, no. 8, pp. 4729-4743, 2013.

[24] W. Zhou, A. C. Bovik, H. R. Sheikh and E. P. Simoncelli, "Image quality assessment: from error visibility to structural similarity", *IEEE Transactions on Image Processing*, vol. 13, no. 4, pp. 600-612, 2004.

[25] L. Zhang, L. Zhang, X. Mou and D. Zhang, "FSIM: A feature similarity index for image quality assessment", *IEEE Transactions on Image Processing*, vol. 20, no. 8, pp. 2378-2386, 2011.

[26] L. L. Biehl, "Hyperspectral images", *purdue.edu*, 1994. [Online]. Available: https://engineering.purdue.edu/~biehl/MultiSpec/hyperspectral.html [Accessed January 02, 2025].